A Novel Non-Hermitian Symmetry Orthogonal Frequency Division Multiplexing System for Visible Light Communications

Xian-Ying Xu, *Student Member, IEEE*, and Dian-Wu Yue, *Senior Member, IEEE*

***Abstract*—This paper proposes a novel non-Hermitian symmetry 2×2 MIMO-OFDM (Multiple Input Multiple Output-Orthogonal Frequency Division Multiplexing) system based on fast Hartley transform (FHT) with unipolar encoding (referred to as HU-OFDM) for visible light communications. The new scheme uses FHT instead of FFT (fast Fourier transform) to process the complex-valued signals reducing the computational complexity and hardware cost and employs two LEDs (light-emitting diodes) to transmit the real and imaginary parts of a complex-valued OFDM signal respectively. Unipolar encoding is applied to the transmitted signal from each LED to ensure non-negative. The restrictions of Hermitian symmetry in traditional optical OFDM systems and real constellation mapping in FHT based optical OFDM systems can be removed simultaneously in the proposed system. Compared with MIMO-ACO/DCO-OFDM system, HU-OFDM has significant performance improvement along with a tremendous decrease in hardware cost and computational complexity. Compared with other non-Hermitian symmetry MIMO-OFDM systems, HU-OFDM has significant advantages in terms of power efficiency, system design flexibility, computational complexity, or hardware cost without losing reliability.**

***Index Terms*—MIMO-OFDM, non-Hermitian, FHT, unipolar encoding, visible light communication.**

I. Introduction

THE OPTICAL signals cannot be affected by the interference of electromagnetic radiation, so optical communication can replace radio frequency (RF) communication in the environment where electromagnetic pollution is serious. As the fourth generation of lighting source, LED has the advantages of high efficiency, energy-saving, and environmental protection. Therein, white LED has become the most competitive source in the lighting field [1]. Visible light communication (VLC) based on white LED can provide both illumination and communication, it has attracted tremendous research interest. Compared with other wireless communications, VLC has been able to achieve very high data rates and possessed unique advantages, such as high security, utmost privacy, and abundant spectrum [2]. A hybrid network of VLC and RF can meet the requirement of a fast, secure, and highly reliable wireless connection in 6 G (the sixth generation). Therefore, VLC is a promising candidate for future 6 G networks, and will play an increasingly important role in wireless short-distance transmission [3].

The modulation bandwidth of a single LED is only a few MHz, which is a major factor limiting the transmission rate of VLC. To satisfy the need of high-speed data rate, OFDM is introduced into indoor VLC. OFDM is a multi-carrier modulation technology, which can effectively combat both the inter-symbol interference of wireless channels and the distortion caused by the nonlinear frequency response of LED. However, the traditional OFDM symbols are bipolar complex signals. The VLC systems use intensity modulation/ direct detection (IM/DD), which requests OFDM symbols to be real and positive. Therefore, it is necessary to investigate approaches to convert bipolar OFDM symbols into unipolar ones. Scholars have conducted a lot of research on unipolar OFDM modulation techniques suitable for VLC systems. The typical schemes are based on inverse fast Fourier transform (IFFT) to implement OFDM, such as DCO-OFDM (DC-biased optical OFDM) [4], ACO-OFDM (Asymmetrically clipped optical OFDM) [5], U-OFDM (Unipolar-OFDM) [6], Flip-OFDM [7], and PAM-DMT (Pulse amplitude modulated discrete multitone) [8]. In [9], the performances of spectrum and energy efficiency of typical unipolar schemes were analyzed. Simulation results showed that DCO-OFDM achieves the highest spectral efficiency but poor power efficiency, and U-OFDM was optimal. Later, some researchers have put forward enhanced and hybrid optical OFDM schemes to further improve the spectral efficiency, such as eU-OFDM (enhanced U-OFDM) [10], LACO-OFDM (Layered ACO-OFDM) [11], ADO-OFDM (Asymmetrically clipped DC-biased optical OFDM) [12], HACO-OFDM (Hybrid ACO-OFDM) [13], and AAO-OFDM (Asymmetrically clipped absolute value optical OFDM) [14]. These enhanced schemes pursued advanced spectral efficiency as close as to that of DCO-OFDM at the cost of computational complexity, in which IFFT/FFT of high computational complexity is still adopted to realize the modulation/demodulation of OFDM. Furthermore, the symbols in frequency subcarriers are expected to have Hermitian symmetry to get real signals, which halves the spectral efficiency before unipolar processing. Unipolar schemes which

Manuscript received August 6, 2021; revised September 25, 2021; accepted October 8, 2021. Date of publication October 14, 2021; date of current version October 27, 2021. *(Corresponding author: Dian-Wu Yue.)*

Xian-Ying Xu is with the College of Information Science and Technology, Dalian Maritime University, Liaoning 116024, China, and also with the College of Electrical Engineering, Dalian University of Science and Technology, Liaoning 116024, China (e-mail: xuxianying@dlmu.edu.cn).

Dian-Wu Yue is with the College of Information Science and Technology, Dalian Maritime University, Liaoning 116024, China (e-mail: dwyue@dlmu.edu.cn).

Digital Object Identifier 10.1109/JPHOT.2021.3120025

do not claim Hermitian symmetry include PM-OFDM (Position modulating OFDM) [15] and P-OFDM (Polar OFDM) [16]. However, the spectral efficiency of PM-OFDM is only half of that of DCO-OFDM, and the complexity of P-OFDM is high due to coordinate system transformation and separate transmission of amplitude and phase.

Apart from the above non-Hermitian symmetry OFDM schemes, some researchers have investigated non-Hermitian symmetry MIMO-OFDM systems, using LEDs to distinguish the real/imaginary part or positive/negative part of signals in the time domain. These methods can enhance the performance owing to that the subcarriers can be more fully used. The idea of using LED to distinguish polarity of signals first appeared in NDC-OFDM (Non-DC-biased OFDM) to improve power efficiency and spectral efficiency [17]. However, NDC-OFDM still employed FFT/IFFT and required Hermitian symmetry. Based on this, non-Hermitian symmetry MIMO-OFDM systems were raised [18]–[20]. In [18], NHS-OFDM (Non-Hermitian Symmetry OFDM) transmitted the real and imaginary parts of complex OFDM symbols separately. DC (direct current) bias was added to both real-valued signals to ensure non-negative, which resulted in a loss of power efficiency. Generally, the bias was not to be excessive, the peaks of the negative-going signal would be clipped, which would add a clipping noise component. Besides, the complexity of NHS-OFDM is high because of FFT. In [19], SH-OFDM (Spatial Modulation with DHT-Based OFDM) was presented to lower computational complexity utilizing FHT. Two LEDs were deployed to transmit positive and negative parts of signals respectively. Without Hermitian symmetry and DC bias, SH-OFDM was spectral and power efficient. However, real constellation mapping was demanded to get real signals. In [20], GLIM-OFDM (Generalized LED Index Modulation Optical OFDM) used two pairs of LEDs to transmit the real and imaginary parts of complex OFDM symbols, in which each pair of LEDs transmitted positive and negative parts of real/imaginary part respectively. GLIM-OFDM still used FFT and required at least 4 LEDs, leading to high hardware cost and computational complexity. Soon afterward, [21], [22] generalized the number of LEDs and presented more general MIMO-GLIM models. [23] combined GLIM-OFDM with P-OFDM and proposed a polar fully generalized LED-indexed OFDM to further boost spectral efficiency.

Compared with Fourier transform, Hartley transform can increase the computing speed and decrease the computational complexity for omitting the calculation of imaginary part. The forward and inverse transformations of FHT are the same, so modulation and demodulation can be realized by the same generator which saves the hardware cost [24]. Therefore, some researchers considered imposing FHT on VLC systems to reduce the computational complexity and hardware cost [25], [26]. More importantly, using FHT can avoid the Hermitian symmetry constraint if the input symbols of FHT adopt the real constellation mapping, such as BPSK (Binary Phase Shift Keying) or PAM (Pulse Amplitude Modulation), which will in return astricts the applicability of FHT. However, according to [27], FHT can be applied in the complex domain and will bring lots of advantages because of real data calculations.

In this paper, a novel non-Hermitian symmetry optical OFDM system based on FHT (referred to as HU-OFDM) is proposed. The new system removes the restriction of real constellation mapping in [19] and adopts a more favorable complex constellation mapping mode like QAM. In HU-OFDM, two LEDs transmit the real and imaginary parts separately, and the unipolar encoding method is used to both signals to guarantee non-negative. On the one hand, since no DC bias is added, the power efficiency is significantly enhanced compared with [18]. On the other hand, compared with [20], the hardware cost and computational complexity can be decreased and the flexibility of system design can be increased without losing reliability.

This paper focuses on investigating a new non-Hermitian symmetry optical OFDM system (HU-OFDM), and gives a generalized MIMO-HU system aiming at the practical irradiation environment. The rest of the paper is organized as follows: Section II describes the model and principle of HU-OFDM. In Section III, we give theoretical analysis of BER performance for HU-OFDM. We compare the HU-OFDM with ACO/DCO-OFDM in 2×2 MIMO system in Section IV and make comparisons of the existing non-Hermitian symmetry optical OFDM schemes in Section V. Finally, Section VI concludes the study.

II. System Model

A. HU-OFDM

The system model of HU-OFDM is illustrated in Fig. 1. The input bit stream is mapped by an *M*-QAM modulator into a complex sequence where $\mathbf{X}_k = (X_0, X_1, X_2, \ldots, X_{N-1}), k = 0, 1, \ldots, N-1$. After the N-IFHT operation, the real and imaginary parts of the time-domain signals are separated to get $\mathbf{x}_{\mathrm{R}}$ and $\mathbf{x}_{\mathrm{I}}$ relatively, which are still bipolar and will be imposed unipolar encoding to obtain non-negative signals for VLC. With $R(k)$ and $I(k)$ representing the real and imaginary part of $X(k)$ respectively, and $r(n)$ and $i(n)$ representing the real and imaginary parts of $x(n)$ respectively, N-FHT / N-IFHT for complex-valued signals can be defined as [24], [27]

$$\begin{aligned}
\text{FHT}: x(n) &= \frac{1}{\sqrt{N}} \sum_{k=0}^{N-1} R(k)\text{cas}(2\pi kn/N) \\
&\quad + j\frac{1}{\sqrt{N}} \sum_{k=0}^{N-1} I(k)\,\text{cas}'\,(2\pi kn/N)\,, \\
&\quad 0 \le n \le N-1 \\
\text{IFHT}: X(k) &= \frac{1}{\sqrt{N}} \sum_{n=0}^{N-1} r(n)\text{cas}(2\pi kn/N) \\
&\quad + j\frac{1}{\sqrt{N}} \sum_{k=0}^{N-1} i(n)\,\text{cas}'\,(2\pi kn/N)\,, \\
&\quad 0 \le k \le N-1
\end{aligned} \tag{1}$$

with

$$\text{cas}\,(2\pi kn/N) = \cos\,(2\pi kn/N) + \sin\,(2\pi kn/N) \tag{2}$$

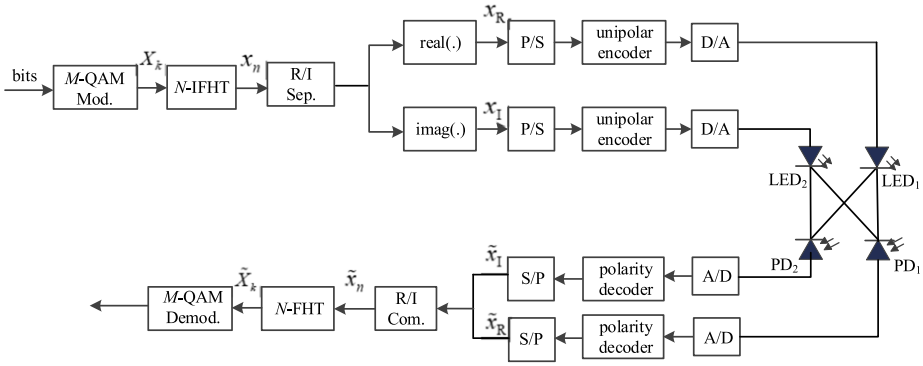

QAM Mod.: quadrature amplitude modulation; QAM Demod.: quadrature amplitude Demodulation;
IFHT: inverse fast Hartley transform; FHT: fast Hartley transform;
P/S: parallel-serial conversion; S/P: serial-parallel conversion;
D/A: digital-to-analog conversion; A/D: analog-to-digital conversion;
R/I Sep.: real and imaginary parts separator; R/I Com.: real and imaginary parts combiner

Fig. 1. Block diagram of HU-OFDM system.

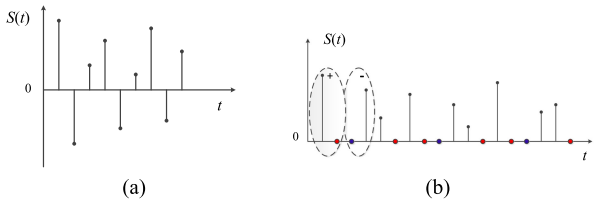

Fig. 2. Schematic diagram of unipolar coding principle. (a) Original bipolar samples, (b) Coded non-negative samples.

and cas' is the complementary function of cas in order to analyze given functions that are complex, which is defined by

$$\mathrm{cas}'\left(2\pi kn/N\right) = \cos\left(2\pi kn/N\right) - \sin\left(2\pi kn/N\right) \tag{3}$$

The rule of unipolar coding is to encode one sample into a pair of new samples, one of which retains the absolute value of the original sample, and the other represents its polarity sign with '0'. If the original sample is positive, the first sample of the new pair is set the absolute value of the original sample, and the second sample is set '0'. If, on the other hand, '0' is ahead of the absolute value. All samples of OFDM symbols encoded in this way are non-negative. Fig. 2 shows how the bipolar samples in Fig. 2(a) are encoded into non-negative samples in Fig. 2(b).

B. Channel Model

HU-OFDM employs a 2×2 MIMO structure, and the channel matrix can be expressed as

$$\mathbf{H} = \begin{bmatrix} h_{11} & h_{12} \\ h_{21} & h_{22} \end{bmatrix} \tag{4}$$

where $h_{r,t}$ is the channel gain from the tth LED to the rth PD. [28] has proved that light intensity of the LOS (line of sight) component is much higher than that of the strongest diffuse component, so it is reasonable to only consider the LOS channel here, which can be described as [29]

$$h_{r,t} = \frac{(\beta+1)\,A_r}{2\pi d^2}\cos^{\beta}(\phi)\,T_s(\psi)\,g_c(\psi)\cos(\psi)\,\mathrm{rect}\left(\frac{\psi}{\Psi_c}\right) \tag{5}$$

with

$$\mathrm{rect}(x) = \begin{cases} 1, & |x| \le 1 \\ 0, & |x| > 1 \end{cases} \tag{6}$$

$$d = \|\mathbf{r}_l - \mathbf{r}_p\| \tag{7}$$

$$\cos\phi = \hat{\mathbf{n}}_l \cdot (\mathbf{r}_p - \mathbf{r}_l)/d \tag{8}$$

$$\cos\psi = \hat{\mathbf{n}}_p \cdot (\mathbf{r}_l - \mathbf{r}_p)/d \tag{9}$$

where β is the order of the Lambertian emission, A_r is the active area of PD, d is the distance between the tth LED and the rth PD, and ϕ and ψ denote the angles of irradiance and incidence respectively.Ψ_c is the field-of-view (FOV) of the PD. $T_s(\psi)$ and $g_c(\psi)$ denote the optical filter gain and the concentrator gain, which are assumed to be unity in this work. $\mathbf{r}_l$ is the position vector of LED, and $\hat{\mathbf{n}}_l$ is the LED's unit-length orientation vector. $\mathbf{r}_p$ is the position vector of PD, and $\hat{\mathbf{n}}_p$ is the PD's normal vector.

C. Detection of HU-OFDM

At the receivers, the received signal can be expressed as

$$\mathbf{y} = \mathbf{H}\mathbf{x} + \mathbf{n} \tag{10}$$

where $\mathbf{x} = [x_{\mathrm{R}}, x_{\mathrm{I}}]^{\mathrm{T}}$, $\mathbf{n}$ is additive white Gaussian noise (AWGN), and δ_{n}^2 is its variance. In this study, we consider the average electrical SNR at each received unit, which is defined as

$$\mathrm{SNR} = \frac{P_{\mathrm{s,ele}}}{\delta_{\mathrm{n}}^2} \tag{11}$$

where $P_{\mathrm{s,ele}} = \mathrm{E}\{x^2\}$ is the received power at a PD in the electrical domain for a given signal x, and $\mathrm{E}\{\}$ represents expectations.

ZF equalizer is used to recover the transmitted signal as

$$\tilde{\mathbf{x}} = \mathbf{H}^{-1}\mathbf{y} = \mathbf{x} + \mathbf{H}^{-1}\mathbf{n} \tag{12}$$

Then the polarity decoders compare the amplitudes of each pair of samples received by each PD. The one with higher amplitude will be identified as the absolute value of the original sample, and the other one will be considered as the polarity sign and discarded. More specifically, if the amplitude of the first sample is larger, the first sample is considered to be the value-sample, the second sample is the polarity sign, and the original sample is determined to be positive with the value of the first sample. By contrast, If the amplitude of the first sample is smaller, the first sample is considered to be the polarity sign, the second sample is the value one, and the original sample is discriminated to be negative with the opposite value of the second sample. In this way, the bipolar OFDM signal before encoding can be demodulated as $\tilde{\mathbf{x}} = [\tilde{x}_{\mathrm{R}}, \tilde{x}_{\mathrm{I}}]^{\mathrm{T}}$, where $\tilde{x}_{\mathrm{R}}$ and $\tilde{x}_{\mathrm{I}}$ represent the real and imaginary parts respectively. Then the complex sequence can be combined by $\tilde{x}_n = \tilde{x}_{\mathrm{R}} + j\tilde{x}_{\mathrm{I}}$, which will be further processed by N-FHT to get the frequency-domain signal $\tilde{\mathbf{X}}_k$. Finally, the received bitstream data is generated after M-QAM demodulator.

III. BER Analysis for HU-OFDM

The bit error rate of HU-OFDM involves two estimation processes: 1) the estimation of polarity detection at the receivers, and 2) the estimation of transmitted symbols. To compute the overall probability of error P_e, we assume P_c to be the probability of retrieved bits being correct. Thus, we have

$$P_e = 1 - P_c \tag{13}$$

Let P_a denote the probability of the polarity discrimination being incorrect, and let P_b be the probability that the transmitted QAM symbols estimate is incorrect. Let $P_{b|P_a}$ be the probability of the demodulated bits error in the case of that polarity discrimination is incorrect. Then P_c and P_e can be written as

$$P_c = (1 - P_a)(1 - P_b) + P_a\left(1 - P_{b|P_a}\right) \tag{14}$$

$$P_e = 1 - P_c = P_b - P_aP_b + P_aP_{b|P_a} \tag{15}$$

According to [30], the average bit probability of rectangular QAM under an AWGN channel can be obtained by

$$P_b = \frac{4\left(\sqrt{M}-1\right)}{\sqrt{M}\log_2 M}\,\mathrm{Q}\left(\sqrt{\frac{3\mathrm{SNR}_{\mathrm{Rx}}}{M-1}}\right) \tag{16}$$

where $\mathrm{SNR}_{\mathrm{Rx}}$ represents the electrical signal-to-noise ratio at the receiver side, for HU-OFDM given by

$$\mathrm{SNR}_{\mathrm{Rx,HU}} = \frac{2P_{\mathrm{Rx,HU}}(h_{11}h_{22} - h_{12}h_{21})^2}{(h_{11}^2 + h_{12}^2 + h_{21}^2 + h_{22}^2)\,\delta_{\mathrm{n}}^2} \tag{17}$$

where $P_{\mathrm{Rx,HU}}$ is the average electrical power of the received signal after polarity decoding, and let $P_{\mathrm{Tx,HU}}$ be the average electrical power of the transmitted signal. Then it can be concluded that $P_{\mathrm{Rx,HU}} = 2P_{\mathrm{Tx,HU}}$, because polarity decoding removes the sign '0' and doubles the signal power. Thus, (17) can be rewritten as

$$\mathrm{SNR}_{\mathrm{Rx,HU}} = \frac{4P_{\mathrm{Tx,HU}}(h_{11}h_{22} - h_{12}h_{21})^2}{(h_{11}^2 + h_{12}^2 + h_{21}^2 + h_{22}^2)\,\delta_{\mathrm{n}}^2} \tag{18}$$

P_a depends on the rule of polarity distinguish and can be derived as

$$\begin{aligned} P_a &= \frac{1}{2}\,\mathrm{E}\left[P\left(|x_{\mathrm{R}}| \to 0\right) + P\left(|x_{\mathrm{I}}| \to 0\right)\right] \\ &= \frac{1}{2}\,\mathrm{E}\left[\mathrm{Q}\left(\frac{|x_{\mathrm{R}}|}{\delta_{\mathrm{R}}}\right) + \mathrm{Q}\left(\frac{|x_{\mathrm{I}}|}{\delta_{\mathrm{I}}}\right)\right] \end{aligned} \tag{19}$$

with

$$\delta_{\mathrm{R}} = \frac{2\left(h_{12}^2 + h_{22}^2\right)^2\delta_{\mathrm{n}}^2}{\left(h_{11}h_{22} - h_{12}h_{21}\right)^2},\ \delta_{\mathrm{I}} = \frac{2\left(h_{11}^2 + h_{21}^2\right)^2\delta_{\mathrm{n}}^2}{\left(h_{11}h_{22} - h_{12}h_{21}\right)^2} \tag{20}$$

According to the modulation principle of OFDM symbols, each OFDM symbol is the result of the joint action of N-point QAM symbols. Therefore, once the polarity of OFDM symbols is misjudged, the probability of QAM symbols demodulation error cannot be given an accurate mathematical expression, that is $P_{b|P_a}$ cannot be confirmed. Hence, we can only give an approximate solution. Let $P_{b|P_a} \approx 1 - 1/M$, and then we have

$$\begin{aligned} P_e &= P_b - P_aP_b + P_a \cdot P_{b|P_a} \\ &\approx P_b - P_aP_b + \left(1 - \frac{1}{M}\right)P_a \\ &= P_b + P_a\left(1 - \frac{1}{M} - P_b\right) \end{aligned} \tag{21}$$

In this subsection, the analyzed and simulated BER are compared with respect to the average received electrical SNR. Table I lists the key simulation settings. For simplicity, the order of the Lambertian emission β, the optical filter gain $T_s(\psi)$, and the concentrator gain $g_c(\psi)$ are all assumed to be unity. We consider a typical room with a size of 5 m × 5 m × 3 m, where the LEDs are placed on the ceiling and the PDs are located at the height of 1 m. LEDs and PDs are assumed to be facing perpendicularly

TABLE I
Physical Parameters of Simulation Setup

Parameter	Value
Dimensions of the room ($W \times L \times H$)	5m × 5m × 3m
FHT or FFT size	N = 256
Lambertian order	β = 1
Gain of the optical filter	$T_s(\psi)$ = 1
Concentrator gain	$g_c(\psi)$ = 1
Field of View	ψ_{c} = 85°
Area of PD	A_r = 1cm^2
LED Positions	2×2 :
	1: (1.25, 2.5, 3), 2: (3.75, 2.5, 3)
	4×4 :
	1: (1.25, 3.75, 3), 2: (3.75, 3.75, 3)
	3: (3.75, 1.25, 3), 4: (1.25, 1.25, 3)
PD Positions	2×2 :
	1: (2.3, 2.5, 1), 2: (2.7, 2.5, 1)
	4×4 :
	1: (2.3, 2.7 1), 2: (2.7, 2.7, 1)
	3: (2.7, 2.3, 1), 4: (2.3, 2.3, 1)

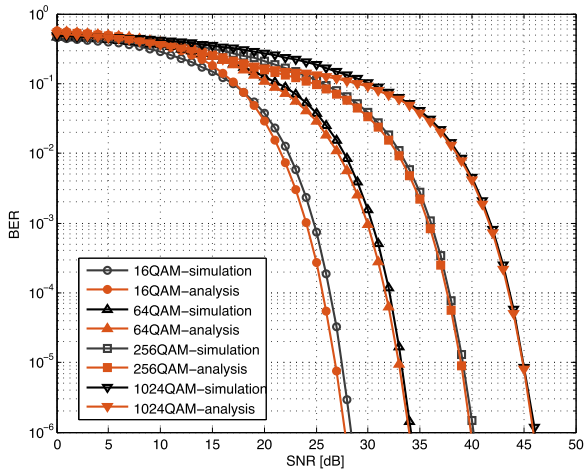

Fig. 3. Analytical and simulated BER of 64QAM, 256QAM, and 1024QAM for HU-OFDM.

down to the floor and upward to the ceiling respectively. The unit-length orientation vector of LEDs is $\hat{\mathbf{n}}_l = (0, 0, -1)$, and the normal vector of PDs is $\hat{\mathbf{n}}_l = (0, 0, 1)$. Unless otherwise stated, LEDs and PDs are symmetrically placed with respect to the central points. In both considered 2×2 and 4×4 MIMO channels, LEDs and PDs are placed in parallel for simulations. We assume LEDs on the ceiling with an equidistant spacing of 2.5 m and PDs with an equidistant spacing of 0.4 m. The 2×2 optical MIMO channel matrix can be calculated referred to equation (5) as

$$\mathbf{H} = 10^{-5} \times \begin{bmatrix} 0.4890 & 0.3419 \\ 0.3419 & 0.4890 \end{bmatrix} \tag{22}$$

The 4×4 optical MIMO channel matrix is calculated as

$$\mathbf{H} = 10^{-5} \times \begin{bmatrix} 0.3307 & 0.2453 & 0.1891 & 0.2453 \\ 0.2453 & 0.3307 & 0.2453 & 0.1891 \\ 0.1891 & 0.2453 & 0.3307 & 0.2453 \\ 0.2453 & 0.1891 & 0.2453 & 0.3307 \end{bmatrix} \tag{23}$$

Fig. 3 presents the simulation and analytical BER of 64QAM, 256QAM, and 1024QAM for HU-OFDM, and the results are in close agreement. As depicted in Fig. 3, the larger the modulation order is, the closer the theoretical values are to the simulation results. For 16QAM and 64QAM, analytical values are slightly lower than simulated ones. This may because the assumed $P_{b|P_a} \approx 1 - 1/M$ is smaller than it is, thus the theoretical values are mildly better than the simulation results. However, the analyzed BER results match the Monte Carlo simulation results at high SNR, especially for high order constellation modulation. In this case, we believe that the energy of the OFDM symbol is big enough that the value of P_a is so small that $P_{b|P_a}$ does not affect the results significantly. Meanwhile, the error probability of QAM symbols P_b is much larger than P_a, thus P_e is more approximately equal to P_b. The gap between P_a and P_b is so great that the inaccuracy of $P_{b|P_a}$ does not affect the results significantly. Therefore, the theoretical values and the simulation results are almost equivalent.

IV. Comparison of HU-OFDM and MIMO-ACO/DCO-OFDM

HU-OFDM avoids Hermitian symmetry enhancing the spectral efficiency, while unipolar coding doubles the frame in the time domain. Therefore, the spectral efficiency of HU-OFDM with M-QAM constellation is given by

$$\eta_{\text{HU-OFDM}} = \frac{1}{2}\log_2 M(\text{bits/s/Hz}) \tag{24}$$

Hermitian symmetry should be imposed in ACO-OFDM and DCO-OFDM, in the meanwhile, ACO-OFDM only modulates the odd subcarriers and DCO-OFDM requires DC bias which will result in spectrum loss and poor power efficiency respectively. The spectral efficiency of ACO-OFDM and DCO-OFDM can be given by

$$\eta_{\text{ACO-OFDM}} = \frac{1}{4}\log_2 M(\text{bits/s/Hz}) \tag{25}$$

$$\eta_{\text{DCO-OFDM}} = \frac{1}{2}\log_2 M(\text{bits/s/Hz}) \tag{26}$$

Compared with ACO-OFDM, the spectral efficiency of HU-OFDM is twice that of ACO. Compared with DCO, the spectral efficiency of HU-OFDM is equal to that of DCO, while DCO has poor power efficiency because of DC bias. For more fair comparisons, HU-OFDM should be compared with ACO-OFDM and DCO-OFDM in 2×2 MIMO system illustrated in Fig. 4. MIMO-ACO/DCO-OFDM is equipped with two pairs of transmitters and receivers resulting in high computational complexity.

The BER performance comparison of HU-OFDM and MIMO-ACO/DCO-OFDM is simulated and the results are showed in Fig. 5 and Fig. 6. The DC bias of MIMO-DCO-OFDM is set to 7 dB and 13 dB. For fair comparison, the relationship of constellation sizes of HU-OFDM and two parallel ACO/DCO-OFDMs should satisfy $M_{\text{HU}} = \sqrt{M_{\text{ACO1}} \cdot M_{\text{ACO2}}} = M_{\text{DCO1}} \cdot M_{\text{DCO2}}$.

As shown in Fig. 5, HU-OFDM performs better than MIMO-ACO-OFDM in terms of BER. At BER $= 10^{-5}$, the power requirement of HU-OFDM is at least 2.5 dB less than that of MIMO-ACO-OFDM for all the presented cases under the same spectral efficiency. From Fig. 6, it can be concluded that the performance of MIMO-DCO-OFDM depends on the DC bias. When the DC bias is small, the negative-going signal will be clipped adding a clipping noise component. As the modulation order increases, the clipping noise increases and finally leads to floor effect as the simulation result shown for MIMO-DCO-OFDM with 16QAM modulation and 7 dB. The DC bias of 13 dB can satisfy the requirement of attaining a non-negative signal but resulting in tremendous power efficiency loss. Both the MIMO-DCO-OFDM with 7 dB and 13 dB perform worse than HU-OFDM. At BER $= 10^{-5}$, the power requirement of HU-OFDM is at least 5 dB less than that of MIMO-DCO-OFDM for all the presented cases under the same spectral efficiency.

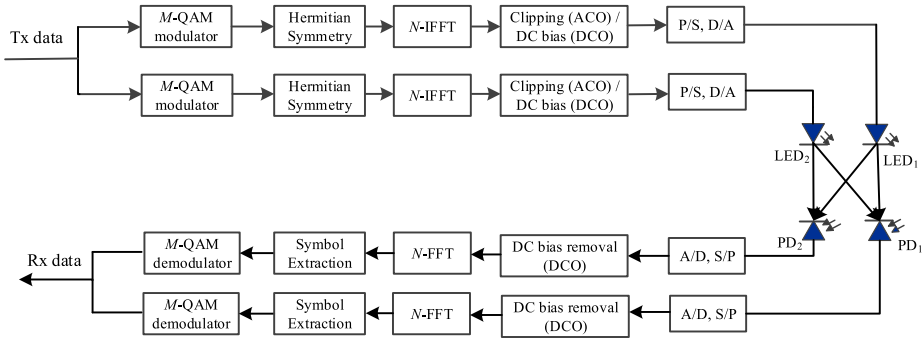

Fig. 4. Block diagram of the MIMO-ACO/DCO-OFDM system.

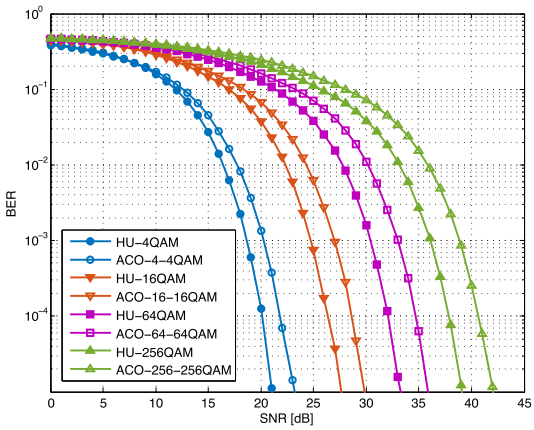

Fig. 5. BER performance comparison of HU-OFDM and MIMO-ACO-OFDM.

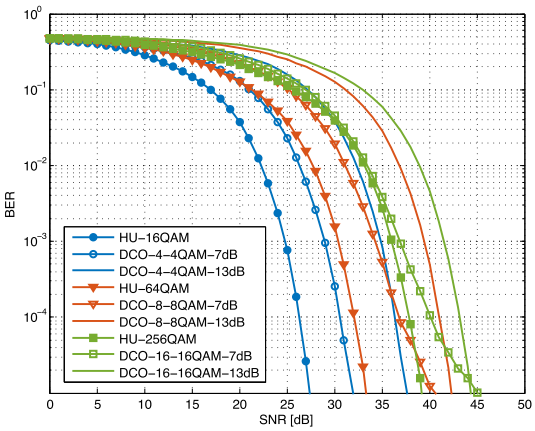

Fig. 6. BER performance comparison of HU-OFDM and MIMO-DCO-OFDM.

V. Comparison of Non-Hermitian OFDMs

A. HU-OFDM Vs. NHS-OFDM

The BER of HU-OFDM and NHS-OFDM (with DC bias of 7 dB or 13 dB) are simulated in the premise of reaching the same spectral efficiency, the results are shown in Fig. 7. Since the frame length is doubled during the unipolar coding process of the HU-OFDM transmitter, the spectral efficiency is lost by half. Therefore, the relationship of constellation size between

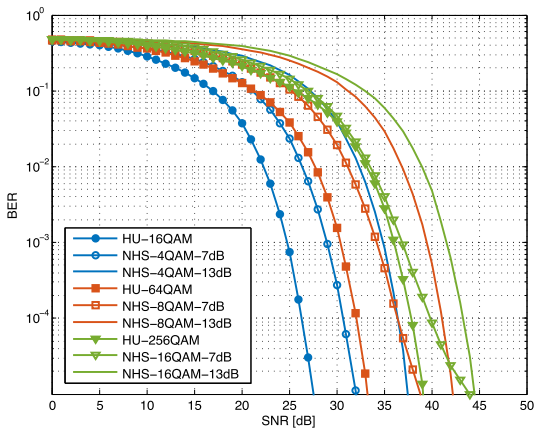

Fig. 7. BER performance comparison between HU-OFDM and NHS-OFDM.

NHS-OFDM and HU-OFDM is $M_{\mathrm{NHS}} = \sqrt{M_{\mathrm{HU}}}$. The BER performance of HU-OFDM is better than that of the NHS-OFDM system, and it also indicates that HU-OFDM has higher power efficiency. This is because

For NHS-OFDM, the SNR at the receiver side is

$$\mathrm{SNR}_{\mathrm{Rx,NHS}} = \frac{2P_{\mathrm{Rx,NHS}}\left(h_{11}h_{22} - h_{12}h_{21}\right)^2}{\left(h_{11}^2 + h_{12}^2 + h_{21}^2 + h_{22}^2\right)\delta_{\mathrm{n}}^2} \tag{27}$$

where $P_{\mathrm{Rx,NHS}}$ is the average electrical power of the received signal after removing the DC bias. Let $P_{\mathrm{Tx,NHS}}$ be the average electrical power of the transmitted signal after adding DC bias. Its obvious that $P_{\mathrm{Rx,NHS}} < P_{\mathrm{Tx,NHS}}$. Thus, we have

$$\mathrm{SNR}_{\mathrm{Rx,NHS}} < \frac{2P_{\mathrm{Tx,NHS}}\left(h_{11}h_{22} - h_{12}h_{21}\right)^2}{\left(h_{11}^2 + h_{12}^2 + h_{21}^2 + h_{22}^2\right)\delta_{\mathrm{n}}^2} \tag{28}$$

combined with (18), there has

$$\mathrm{SNR}_{\mathrm{Rx,NHS}} < \frac{1}{2}\mathrm{SNR}_{\mathrm{Rx,HU}} \tag{29}$$

It can be verified that, with the same average electrical power at the transmitter side (i.e. $P_{\mathrm{Tx,NHS}}$), HU-OFDM provides better BER performance than NHS-OFDM with the same spectral efficiency. NHS-OFDM systems sacrifice some power efficiency due to the need for DC bias. However, the BER performance difference between NHS-OFDM and HU-OFDM is not constant. Because for different modulation orders, NHS-OFDM

will generate different clipping noise even when a fixed DC bias is selected. And as the modulation order increases or DC bias decreases, the clipping noise will increase significantly, which dominates the performance and finally leads to a bad BER. Moreover, it can be observed that the BER performance of NHS-OFDM in Fig. 7 matches with MIMO-DCO-OFDM in Fig. 6. This is because that we employ symmetric LEDs/PDs located in the center of the ceiling or receiving plane for simulation. [18] indicated that SNR values were the same for MIMO-DCO-OFDM and NHS-OFDM if the receivers were located in the center of the receiving plane.

B. HU-OFDM Vs. SH-OFDM

SH-OFDM system also has polarity discrimination and symbol demodulation operations at the receivers. Therefore, we can get

$$P_{a,\mathrm{SH}} = \frac{1}{2}\,\mathrm{E}\left[P\left(x^{+}\to 0\right)+P\left(\left|x^{-}\right|\to 0\right)\right] = \frac{1}{2}\,\mathrm{E}\left[\mathrm{Q}\left(\frac{x^{+}}{\delta_{\mathrm{SH}}}\right)+\mathrm{Q}\left(\frac{|x^{-}|}{\delta_{\mathrm{SH}}}\right)\right] \tag{30}$$

with

$$\delta^2_{\mathrm{SH}} = \frac{\left(h^2_{11}+h^2_{12}+h^2_{21}+h^2_{22}\right)^2\delta^2_{\mathrm{n}}}{\left(h_{11}h_{22}-h_{12}h_{21}\right)^2} \tag{31}$$

where x^{+} and x^{-} represents the positive and negative values of the signal in the time domain.

Then the SNR of SH-OFDM at the receiver side can be expressed as

$$\mathrm{SNR}_{\mathrm{Rx,SH}} = \frac{2P_{\mathrm{Rx,SH}}\left(h_{11}h_{22}-h_{12}h_{21}\right)^2}{\left(h^2_{11}+h^2_{12}+h^2_{21}+h^2_{22}\right)\delta^2_{\mathrm{n}}} = \frac{2P_{\mathrm{Tx,SH}}\left(h_{11}h_{22}-h_{12}h_{21}\right)^2}{\left(h^2_{11}+h^2_{12}+h^2_{21}+h^2_{22}\right)\delta^2_{\mathrm{n}}} \tag{32}$$

The average bit probability of PAM under an AWGN channel can be obtained by [31]

$$P_b = \frac{2\left(M-1\right)}{M\log_2 M}\,\mathrm{Q}\left(\sqrt{\frac{6\mathrm{SNR}_{\mathrm{Rx}}}{M^2-1}}\right) \tag{33}$$

For fairness, the relationship of constellation size between SH-OFDM and HU-OFDM is set to be $M_{\mathrm{SH}} = \sqrt{M_{\mathrm{HU}}}$. Under the same average electrical power at the transmitter side, SH-OFDM and HU-OFDM have the same P_a and P_b, which corresponds to the same BER theoretically. Simulated comparisons of the BER performance of HU-OFDM and SH-OFDM are shown in Fig. 8. We can observe that the BER performance of HU-OFDM is nearly the same as SH-OFDM. However, HU-OFDM removes the restriction of using real constellation mapping in SH-OFDM and employs complex constellation mapping (such as QAM) to modulate symbols in the frequency domain. As recommended by IEEE 802.11ac standard, in order to improve the data rate for next-generation optical wireless access networks, it is necessary to use high order QAM signals [32].

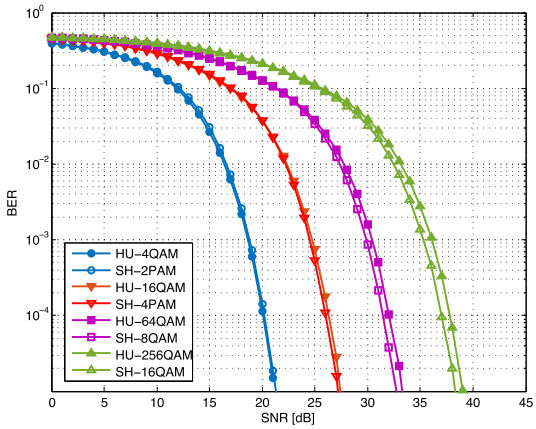

Fig. 8. BER performance comparison of HU-OFDM and SH-OFDM.

C. MIMO-HU Vs. GLIM-OFDM

1) Generalized MIMO-HU System: In this section, the 2×2 HU-OFDM system discussed in Section II is extended to a generalized MIMO system with more than 2 LEDs like [33] did to NHS-OFDM, and the system block diagram is presented in Fig. 9. Without loss of generality, we consider an indoor VLC environment with $2N$ LEDs and $2N$ PDs. These $2N$ LEDs are divided into N pairs, and each pair of LEDs is driven by the two outputs of an HU-OFDM modulator transmitting the real and imaginary parts of OFDM symbols. The average BER of MIMO-HU can be computed as

$$\mathrm{BER} = \frac{1}{N}\sum_{i=1}^{N} P_{e_i} \tag{34}$$

where P_{e_i} represents the bit error rate of the ith HU-OFDM subsystem.

2) Simulation Results: Since GLIM-OFDM is a 4×4 system, let N=2 in the generalized MIMO-HU system for fair comparisons. Two groups of parallel HU-OFDM are used to constitute a 4×4 system and compared with GLIM-OFDM. The relationship of constellation size between GLIM-OFDM and 2HU-OFDM is chosen to be $M_{\mathrm{HU1}}\cdot M_{\mathrm{HU2}} = M^2_{\mathrm{GLIM}}$ to ensure the same spectral efficiency. The total information energy of two HU-OFDM should be the same as that of GLIM-OFDM. Let the information energy of each HU-OFDM be half of that of GLIM-OFDM, and set M_{HU1}=$M_{\mathrm{HU2}} = M_{\mathrm{GLIM}}$.

The simulation results are illustrated in Fig. 10. It can be seen that 2HU-OFDM performs as well as GLIM-OFDM, while 2HU-OFDM employs FHT reducing computational complexity and hardware cost significantly. In the meanwhile, the selection of constellation size in 2HU-OFDM is more flexible, and the energy distribution of 2HU-OFDM signals can be adjusted to meet the actual requirements, such as indoor lighting distribution. In summary, 2HU-OFDM outperforms GLIM-OFDM in terms of design flexibility without sacrificing reliability.

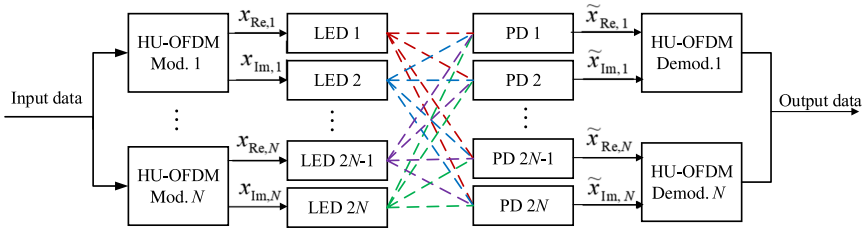

Fig. 9. Block diagram of generalized MIMO-HU system.

TABLE II
COMPARISONS OF NON-HERMITIAN SYMMETRIC OPTICAL OFDM SYSTEMS AND 2×2 MIMO-OFDM SYSTEMS

Optical OFDM Scheme	HU-OFDM	NHS-OFDM	SH-OFDM	GLIM-OFDM	MIMO-ACO-OFDM	MIMO-DCO-OFDM
Based transform	FHT	FFT	FHT	FFT	FFT	FFT
Restriction in constellation mapping	No	No	Yes	No	No	No
Constellation form	Complex (M-QAM)	Complex (M-QAM)	Real (BPSK, M-PAM)	Complex (M-QAM)	Complex (M-QAM)	Complex (M-QAM)
Constellation size	M	M	$\sqrt{M}$	M	M	M
Spectral efficiency (bits/s/Hz)	$\frac{1}{2}\log_2 M$	$\log_2 M$	$\frac{1}{2}\log_2 M$	$\log_2 M$	$\frac{1}{2}\log_2 M$	$\log_2 M$
Minimum required LEDs number	2	2	2	4	2	2
Hermitian symmetry	Not required	Not required	Not required	Not required	Required	Required
DC bias	Not required	Required	Not required	Not required	Not required	Required
Power efficiency	high	low	high	high	high	low
Computational complexity	low	high	low	high	very high	very high
Hardware cost	low	high	low	high	very high	very high
SNR(dB) ($\text{BER}=10^{-4}$,η=2bits/s/Hz)	26.49 (2HU-OFDM: 32.48)	30.82 (DC=7dB) 36.65 (DC=13dB)	26.07	32.10	28.78	30.79 (DC=7dB) 36.74 (DC=13dB)

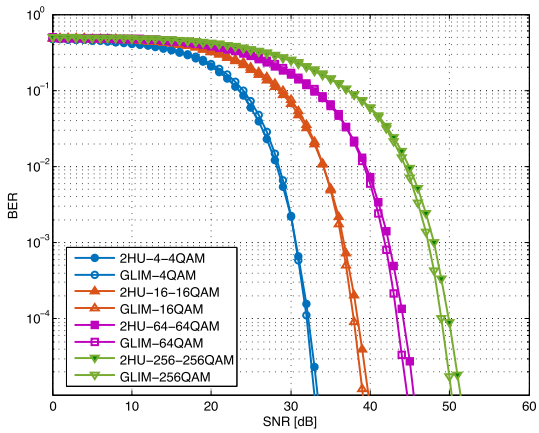

Fig. 10. BER performance comparison of 2HU-OFDM and GLIM-OFDM.

D. Comparisons of Non-Hermitian Symmetry Optical OFDM Systems and MIMO-OFDM Systems

Table II shows the comparisons of HU-OFDM with several other non-Hermitian symmetric optical OFDM schemes and MIMO-ACO/DCO-OFDM (2×2 MIMO). Since the Hartley transform and its inverse form are the same, the modulation and demodulation of the transmitter and receiver can be realized by the same generator, which saves the hardware cost of HU-OFDM significantly. The computational cost of FHT can be saved about 36% compared with FFT [34]. Moreover, FHT allows applying more effective PAPR reduction techniques without the constraint of Hermitian symmetry required by FFT, and with high order constellation modulation, FHT can significantly improve the bit error performance [35]. MIMO-ACO/DCO-OFDM systems have the highest hardware cost and computational complexity because of two sets of IFFT/FFT converter in transmitter/receiver. And MIMO-ACO/DCO-OFDM systems require Hermitian symmetry setting. The computational complexity of HU-OFDM is reduced to nearly half that of NHS-OFDM due to employing FHT, and the power efficiency of HU-OFDM is higher than NHS-OFDM since no DC bias. Compared with SH-OFDM, HU-OFDM has no increase in complexity and removes the constraint of real constellation mapping allowing a more favorable complex constellation mapping mode like QAM. 2HU-OFDM outperforms GLIM-OFDM in terms of design flexibility, computational complexity and hardware cost. And HU-OFDM and 2HU-OFDM have a negligible loss of power efficiency compared with SH-OFDM and GLIM-OFDM respectively.

VI. CONCLUSION

In this paper, a new non-Hermitian symmetric optical OFDM system (HU-OFDM) based on FHT with unipolar encoding has been presented to meet the high data rate requirement of VLC. Instead of using FFT which was usually deployed in

the traditional optical OFDM schemes, FHT was introduced in HU-OFDM dealing with the complex-valued signals to reduce computational complexity, simplify hardware design and save system cost. Two LEDs are deployed to transmit the real and imaginary parts of a complex-valued OFDM signal respectively. Both power and spectrum efficient unipolar encoding method is adopted to obtain the positive signal. The restrictions of Hermitian symmetry in traditional optical OFDM systems and real constellation mapping in FHT based optical OFDM systems can be removed simultaneously in the proposed system. Through comprehensive comparison and simulation verification, this paper has proved that HU-OFDM has significant performance improvement along with a tremendous decrease in hardware cost and computational complexity compared with MIMO-ACO/DCO-OFDM systems. And HU-OFDM performs better than other non-Hermitian symmetric OFDM schemes with respect to power efficiency, design flexibility, or system cost. Besides, the HU-OFDM system was extended to a generalized MIMO-HU system, which was more suitable for indoor illumination environments with multiple LEDs.

REFERENCES

[1] N. Bardsley *et al.*, "Solid-state lighting research and development multi-year program plan," in *Proc. DOE SSL R&D Workshop*, Apr. 2014, pp. 5–11.

[2] S. Kumar and P. Singh, "A comprehensive survey of visible light communication: Potential and challenges," *Wireless Pers. Commun.*, vol. 109, no. 2, pp. 1357–1375, 2019.

[3] M. Katz and I. Ahmed, "Opportunities and challenges for visible light communications in 6G," in *Proc. 2nd 6G Wireless Summit*, 2020, pp. 1–5.

[4] O. González, R. Pérez-Jiménez, S. Rodriguez, J. Rabadán, and A. Ayala, "OFDM over indoor wireless optical channel," *IEE P- Optoelectron.*, vol. 152, no. 4, pp. 199–204, Aug. 2005.

[5] J. Armstrong and A. J. Lowery, "Power efficient optical OFDM," *Electron. Lett.*, vol. 42, no. 6, pp. 370–372, 2006.

[6] D. Tsonev, S. Sinanovic, and H. Haas, "Novel unipolar orthogonal frequency division multiplexing (U-OFDM) for optical wireless," in *Proc. IEEE 75th Veh. Technol. Conf.*, 2012, pp. 1–5.

[7] N. Fernando, Y. Hong, and E. Viterbo, "Flip-OFDM for optical wireless communications," in *Proc. IEEE Inf. Theory Workshop*, 2011, pp. 5–9.

[8] S. C. J. Lee, S. Randel, F. Breyer, and A. M. Koonen, "PAM-DMT for intensity-modulated and direct-detection optical communication systems," *IEEE Photon. Technol. Lett.*, vol. 21, no. 23, pp. 1749–1751, Dec. 2009.

[9] X. Y. Xu and D. W. Yue, "Orthogonal frequency division multiplexing modulation techniques in visible light communication," *Chin. Opt.*, vol. 14, no. 3, pp. 516–527, 2021.

[10] D. Tsonev and H. Haas, "Avoiding spectral efficiency loss in unipolar OFDM for optical wireless communication," in *Proc. IEEE Int. Conf. Commun.*, 2014, pp. 3336–3341.

[11] Q. Wang, C. Qian, X. Guo, Z. Wang, D. G. Cunningham, and I. H. White, "Layered ACO-OFDM for intensity-modulated direct-detection optical wireless transmission," *Opt. Exp.*, vol. 23, no. 9, pp. 12 382–12393, 2015.

[12] S. D. Dissanayake and J. Armstrong, "Comparison of ACO-OFDM, DCO-OFDM and ADO-OFDM in IM/DD systems," *J. Lightw. Technol.*, vol. 31, no. 7, pp. 1063–1072, 2013.

[13] B. Ranjha and M. Kavehrad, "Hybrid asymmetrically clipped OFDM-based IM/DD optical wireless system," *IEEE/OSA J. Opt. Commun. Netw.*, vol. 6, no. 4, pp. 387–396, Apr. 2014.

[14] R. Bai, Q. Wang, and Z. Wang, "Asymmetrically clipped absolute value optical OFDM for intensity-modulated direct-detection systems," *J. Lightw. Technol.*, vol. 35, no. 17, pp. 3680–3691, 2017.

[15] A. Nuwanpriya, A. Grant, S.-W. Ho, and L. Luo, "Position modulating OFDM for optical wireless communications," in *Proc. IEEE Globecom Workshops*, 2012, pp. 1219–1223.

[16] H. Elgala and T. D. Little, "Polar-based OFDM and SC-FDE links toward energy-efficient gbps transmission under IM-DD optical system constraints," *IEEE/OSA J. Opt. Commun. Netw.*, vol. 7, no. 2, pp. A 277–A284, Feb. 2015.

[17] Y. Li, D. Tsonev, and H. Haas, "Non-DC-biased OFDM with optical spatial modulation," in *Proc. IEEE 24th Annu. Int. Symp. Pers., Indoor, Mobile Radio Commun.*, 2013, pp. 486–490.

[18] C. Chen, W.-D. Zhong, and D. Wu, "Non-hermitian symmetry orthogonal frequency division multiplexing for multiple-input multiple-output visible light communications," *IEEE/OSA J. Opt. Commun. Netw.*, vol. 9, no. 1, pp. 36–44, Jan. 2017.

[19] Y. Cao, X. Zhou, J. Sun, W. Zhang, and C.-X. Wang, "Optical spatial modulation with DHT-based OFDM in visible light communication systems," in *Proc. 9th Int. Conf. Wireless Commun. Signal Process.*, 2017, pp. 1–5.

[20] A. Yesilkaya, E. Basar, F. Miramirkhani, E. Panayirci, M. Uysal, and H. Haas, "Optical MIMO-OFDM with generalized LED index modulation," *IEEE Trans. Commun.*, vol. 65, no. 8, pp. 3429–3441, Aug. 2017.

[21] M. Le Tran, S. Kim, T. Ketseoglou, and E. Ayanoglu, "LED selection and MAP detection for generalized LED index modulation," *IEEE Photon. Technol. Lett.*, vol. 30, no. 19, pp. 1695–1698, Oct. 2018.

[22] H. S. Hussein and M. Hagag, "Optical MIMO-OFDM with fully generalized index-spatial LED modulation," *IEEE Commun. Lett.*, vol. 23, no. 9, pp. 1556–1559, Sep. 2019.

[23] H. S. Hussein, "Optical polar based MIMO-OFDM with fully generalised index-spatial LED modulation," *IET Commun.*, vol. 14, no. 2, pp. 282–289, Jan. 2020.

[24] R. N. Bracewell, *The Hartley Transform*. Oxford, U.K.: Oxford Univ. Press, 1986.

[25] J. Tang and L. Zhang, "Efficient real-Fourier domain-based color shift keying OFDM implemented with Hartley transform for visible light communication system," in *Proc. IEEE 85th Veh. Technol. Conf.*, 2017, pp. 1–5.

[26] A. W. Azim, Y. Le Guennec, and G. Maury, "Spectrally augmented Hartley transform precoded asymmetrically clipped optical OFDM for VLC," *IEEE Photon. Technol. Lett.*, vol. 30, no. 23, pp. 2029–2032, Dec. 2018.

[27] R. N. Bracewell, "Aspects of the Hartley transform," *Proc. IEEE*, vol. 82, no. 3, pp. 381–387, Mar. 1994.

[28] L. Zeng *et al.*, "High data rate multiple input multiple output (MIMO) optical wireless communications using white LED lighting," *IEEE J. Sel. Areas Commun.*, vol. 27, no. 9, pp. 1654–1662, Dec. 2009.

[29] J. M. Kahn and J. R. Barry, "Wireless infrared communications," *Proc. IEEE*, vol. 85, no. 2, pp. 265–298, Feb. 1997.

[30] K. Cho and D. Yoon, "On the general BER expression of one-and two-dimensional amplitude modulations," *IEEE Trans. Commun.*, vol. 50, no. 7, pp. 1074–1080, Jul. 2002.

[31] A. Goldsmith, *Wireless Communications*. Cambridge, U.K.: Cambridge Univ. Press, 2005.

[32] M. R. N. Babir and P. K. Choudhury, "On the performance of high order QAM signals for analog and digital radio over fiber systems," in *Proc. 4th Int. Conf. Adv. Electr. Eng.*, 2017, pp. 379–382.

[33] C. Chen, W.-D. Zhong, and D. Wu, "On the coverage of multiple-input multiple-output visible light communications," *IEEE/OSA J. Opt. Commun. Netw.*, vol. 9, no. 9, pp. D 31–D41, Sep. 2017.

[34] A. P. Averchenko and B. D. Zhenatov, "Comparison of computational costs of Hartley transform and Fourier transform," in *Proc. Int. Sci.-Tech. Conf. Actual Problems Electron. Instrum. Eng.*, 2016, vol. 1, pp. 436–438.

[35] L. Nadal, M. S. Moreolo, J. M. Fabrega, and G. Junyent, "Comparison of peak power reduction techniques in optical OFDM systems based on FFT and FHT," in *Proc. IEEE 13th Int. Conf. Transparent Opt. Netw.*, 2011, pp. 1–4.